

Control Law Design for Haptic Interfaces to Virtual Reality

Richard J. Adams and Blake Hannaford

Abstract—The goal of control law design for haptic displays is to provide a safe and stable user interface while maximizing the operator's sense of kinesthetic immersion in a virtual environment. This paper outlines a control design approach which stabilizes a haptic interface when coupled to a broad class of human operators and virtual environments. Two-port absolute stability criteria are used to develop explicit control law design bounds for two different haptic display implementations: impedance display and admittance display. The strengths and weaknesses of each approach are illustrated through numerical and experimental results for a three degree-of-freedom device. The example highlights the ability of the proposed design procedure to handle some of the more difficult problems in control law synthesis for haptics, including structural flexibility and noncollocation of sensors and actuators.

Index Terms—Control system human factors, force feedback, haptic display, stability criteria, virtual reality.

I. INTRODUCTION

THE WORD haptic means “of or relating to the sense of touch.” Haptic feedback is a new and relatively unexplored way of conveying information between a human and a computer. A video monitor provides visual information, speakers provide audio information, in an analogous manner, a haptic display conveys kinesthetic information to the operator through the sense of touch. The haptic display generates force feedback cues which may represent the resistance of a virtual wall, the roughness of a virtual texture, or the weight of a virtual mass. Haptic devices come in all shapes and sizes, ranging from large industrial manipulators to motorized desktop mice.

The field of haptics has been led by research applications. Some of the most exciting work is in surgery simulation. The goal is to permit student surgeons to safely practice procedures using haptic and graphical interfaces which accurately reflect real surgical conditions [1], [2]. Another burgeoning area is force feedback in computer-aided design (CAD). By allowing the designer to actually touch the objects under design, haptics may greatly increase efficiency and creativity. It is not surprising that the most rapidly evolving side of haptics is consumer products. The first consumer haptic devices were force feedback joysticks for computer gaming. With the acceptance of standard application programming interfaces (APIs), the number of force feedback enabled computer games has skyrocketed, and new interfaces, such as force feedback steering wheels, have appeared.

Manuscript received September 13, 1999; revised September 20, 2000. Manuscript received in final form August 7, 2001. Recommended by Associate Editor D. W. Repperger.

The authors are with the Department of Electrical Engineering, University of Washington, Seattle, WA 98195-2500 USA.

Publisher Item Identifier S 1063-6536(02)00327-5.

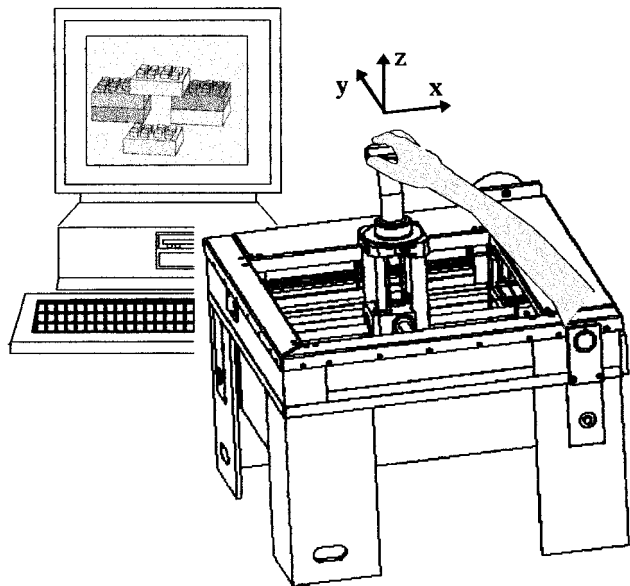


Fig. 1. Excalibur and the virtual building block simulation.

The advent of the force feedback mouse [3] and force feedback enabled graphical user interfaces (GUIs) may eventually bring haptic technology to the majority of computer users' desktops.

The virtual building block (VBB) system is an example of haptic simulation, developed at the University of Washington BioRobotics Laboratory to demonstrate the utility of haptic technology in CAD and virtual prototyping applications. The system currently uses the Excalibur three-axis force display built by Haptic Technologies Inc. of Seattle, WA [4], [5]. Fig. 1 illustrates the simulation. The user can select and manipulate individual blocks or groups of blocks. Haptic feedback represents each object's inertia, prevents objects from impeding on each other, and renders interaction forces when blocks are “snapped” together.

In one sense, haptic interaction is very different from other modes of human-computer interface. In haptic display, there is a bidirectional flow of information, both from the device to the computer and from the computer to the device. The haptic display is not just a “force player,” rendering preset force effects. It is a “force feedback” device which creates forces in response to the user's input. As with any device where feedback is present, the potential for instability exists. Instabilities will at best degrade the quality of the force feedback information to the human operator. In the case of devices with significant inertia and force output, the consequences of instability may be more severe.

The nascent field of controls for haptic displays offers interesting challenges. As with most control problems, there are two

sometimes conflicting goals, performance and stability. Good performance implies forces and velocities experienced by the human operator are nearly identical to those generated by the application software. This is the “transparency” of the haptic interface [6]. The performance of any haptic display is limited at one extreme by how well it can simulate free motion and at the other extreme by how well it can generate rigid constraints. The minimum and maximum achievable impedance of a haptic interface delineates its “impedance range” [7], another useful measure of haptic performance. The inability to render arbitrarily small or large impedance to the human operator is due, in part, to the onset of instability. The stability of a haptic interface is strongly affected by both the application software and the nature of human-device contact. The application software, which we will also refer to as the “virtual environment,” determines what forces are rendered through the haptic display to the human operator. If the application calls for an unachievable level of impedance, for example by creating an excessively rigid virtual wall, the haptic display may oscillate violently. The manner in which the human operator contacts the haptic display also affects the stability of the overall system. With improperly designed controls, instability may ensue when the operator grasps the device very tightly or, conversely, oscillations may occur when the device is released.

In early applications of haptic display, no distinction was made between the virtual environment and the control law for the haptic device. In effect, the virtual environment was the control system. The stiffness and damping of a virtual wall became proportional-plus-derivative feedback gains on device position. Some examples are found in [8]–[10]. This approach has two major drawbacks. First, it is very difficult to ensure that a complex dynamic virtual environment translates into a stabilizing control law for a haptic device. The application software must be tuned and tested extensively, and even then, stability is not assured. Second, since the virtual environment must be tuned for a specific device, the application software must be redesigned if it is to be used with a different haptic display. In other words, a haptic enabled CAD package that works properly with one force feedback mouse may induce instabilities when linked to a different mouse which has slightly less mechanical damping. An improved approach to control law design for haptic displays would separate the problem of device control from the design of application software.

The use of an artificial coupling between the haptic display and the virtual environment was first proposed by Colgate *et al.* [11]. Zilles and Salisbury [12] suggested a similar “god-object” approach which couples a haptic device to a virtual environment through a virtual spring-damper. Adams and Hannaford [13] put the problem of stable haptic simulation into a two-port framework. The two-port approach allows for rigorous stability and performance analysis for a very general class of haptic displays. Virtual couplings may be designed for devices with structural flexibility, force sensing, noncollocated sensors and actuators, and measurement delay.

This paper builds upon the theoretical work presented in [13]. A review of the two-port framework for analysis and design of haptic interfaces precedes the introduction of new developments. Conservatism in previous results is reduced

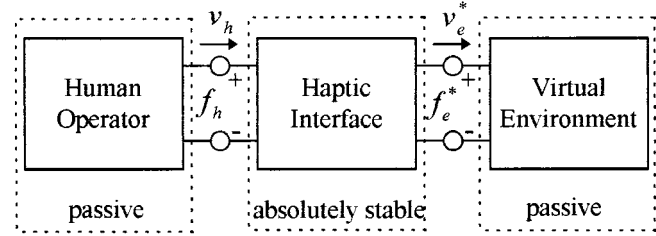


Fig. 2. Network model of haptic simulation.

using a new technique which restricts the assumed human operator impedance to realistic levels. A model for the Excalibur force display is developed, and numerical data provided for a critical design point. The work of [13] is extended to permit regulator and virtual coupling design for a much broader class of haptic displays. Two haptic display implementations are explored, numerically and experimentally, for Excalibur. The strong agreement between theoretical and experimental results highlights the utility of the proposed two-port framework for haptic interface analysis and design.

II. TWO-PORT FRAMEWORK FOR STABILITY AND CONTROL

Two-port methods are rooted in linear circuit theory, where they are used to characterize the effects of different loading conditions on two terminal electrical networks. We can consider a mechanical analog to this electrical two-port, the haptic interface, which is subject to variable loading conditions both at the point of interaction with the human operator and at the point of interaction with the virtual environment. In using this mechanical analog, we substitute velocities for currents in representing flow and forces for voltages in representing effort. The two-port haptic interface model characterizes the exchange of energy between the human operator and the virtual environment. It is useful in studying the stability of the overall system and in describing the performance of the haptic interface. Fig. 2 shows the network model of haptic simulation. The human operator affects the velocity, v_h , and force, f_h , at the physical point of contact with the haptic display. The virtual environment modulates the velocity, v_e^* , and force, f_e^* , at the point of information exchange with the haptic interface. The virtual environment is a digital system. The star superscript indicates that a variable is discrete, defined only at the time of sampling.

In the analysis and design of haptic interfaces, we are interested in a particular representation of the two-port system, known as an *immittance matrix*. A matrix P , which maps the input u to output y , is an immittance matrix characterization of the haptic interface if $y^T u = f_h v_h + f_e^* (-v_e^*)$. There are four ways to form such a matrix. These are the impedance matrix, Z , the admittance matrix, Y , the hybrid matrix, H , and the alternate hybrid matrix, G . Any one of these forms can be formed as an algebraic combination of the elements of any of the others, provide that the matrices exist. By definition, if any one of these matrices is positive real, then all of the others will be as well. The converse is also true. More details on two-port representation can be found in [13], [14].

We will say that the overall haptic simulation is *stable* if, for given human operator and virtual environment impedance, the

resulting characteristic equation has no roots in the right half s -plane and only simple roots on the imaginary axis. Unfortunately, we do not have *a priori* knowledge of the level of human or virtual environment impedance. We would like the haptic simulation to remain stable under any foreseeable variation. A useful notion for handling this issue of robustness is absolute stability. A linear two-port is said to be absolutely stable if there exists no set of passive terminating one-port impedances for which the system is unstable. Thus, if the haptic interface can be made absolutely stable, the haptic simulation will remain stable as long as the human operator and virtual environment are passive.

Llewellyn's stability criteria provide both necessary and sufficient conditions for absolute stability of linear two-ports [14], [15]

- $P(s)$ has no poles in the right half s -plane, only simple poles on the imaginary axis,
- $\text{Re}(p_{11}(s)) \geq 0$ (1)
- $2\text{Re}(p_{11}(s))\text{Re}(p_{22}(s)) \geq |p_{12}(s)p_{21}(s)| + \text{Re}(p_{12}(s)p_{21}(s))$. (2)

Together, the two inequalities imply $\text{Re}(p_{22}(s)) \geq 0$. The satisfaction of the absolute stability criteria for any one of the immittance matrix forms (Z , Y , H , or Z) is necessary and sufficient for them to hold for the other three [14]. By demonstrating that the haptic interface two-port satisfies these criteria, the stability of the system is assured for any level of passive human operator and virtual environment impedance.

Treating energetic interaction between the human arm and a mechanical device as passive appears to be a reasonable assumption. In experimental studies, Hogan found that despite neural feedback within the arm and a high degree of adaptability in the neuromuscular system, the impedance exerted by a human is passive [16]. Requiring that the virtual environment act as a passive operator can be challenging. It is intuitive that the simulation of physically motivated effects (masses, springs, dampers) should obey conservation laws of physics, and thus be passive. However, formulating numerical integration routines which achieve strict adherence to these laws can be difficult. Brown [17] showed that explicit discrete-time passive integration of the equations of motion is impossible. Fortunately, experience has demonstrated that absolutely stable haptic interfaces are very robust when coupled to virtual environments which are "almost" passive [18], [19].

For some haptic interfaces, representing the human operator as an arbitrary passive impedance can be overly conservative. Arbitrary passivity allows for the extreme cases of zero human impedance (no contact) and a perfectly rigid (infinitely stiff) human grasp. If a haptic display has very little mechanical damping, it becomes difficult to achieve any level of performance while maintaining absolute stability. In this case we may want to assume some minimum level of impedance, Z_{\min} , which will be provided by the human operator's contact with the device. This strategy should always be coupled with some form of dead-man's switch since the system may well be unstable if the operator breaks contact with the haptic device.

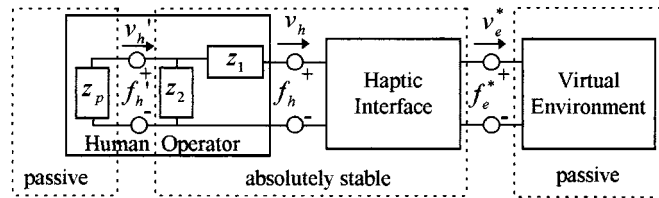


Fig. 3. Human operator impedance model.

If the haptic display implementation includes force sensing at the human-device interface, the stability analysis may be dominated by the unrealistic scenario of infinitely high human stiffness. This conservatism can be abated by postulating a maximum level of impedance Z_{\max} for the human operator. Fig. 3 shows how the analysis model can be modified to include minimum and maximum levels of human impedance. We characterize the human operator in terms of three impedances, Z_p , Z_1 , and Z_2 . Z_p is an arbitrary passive impedance function, $Z_1 = Z_{\min}$, and $Z_2 = Z_{\max} - Z_{\min}$. Notice that when Z_p is zero (short circuit) the resulting human impedance is Z_{\min} . When Z_p is infinite (open circuit), the resulting human impedance is $Z_1 + Z_2 = Z_{\max}$.

The stability conditions in this paper are contingent upon the linearity of the system and the fidelity of linear model. It is possible for nonlinear systems to be treated using a similar passivity-based approach, but this problem is not addressed in the present work. A fairly direct approach to nonlinear problems would be to first apply some form of feedback linearization before performing the linear design discussed here. Structured singular value analysis techniques might be used to analyze the effect of uncertainty in the linear model due to parameter variations and unmodeled dynamics. Unfortunately, these approaches are not currently viable as a synthesis scheme for virtual couplings.

III. EXCALIBUR MODEL

Excalibur is a three degree-of-freedom Cartesian manipulator, designed to act as a haptic interface to virtual or remote environments. Brushless motors provide control forces through a steel cable transmission along three mutually orthogonal translational axes. The user grasps a handle mounted on the end effector as shown in Fig. 1. The device is capable of rendering peak forces of up to 200 N and continuous forces of up to 100 N in each axis over the workspace of $300 \times 300 \times 200$ mm³. The dynamics of the manipulator are a function of the location of the handle within the workspace. All three axes of motion (x , y , z) must be considered. For brevity, we will restrict our attention to a single, worst-case design point for the Excalibur. This is the location at which the device exhibits a structural resonance at the lowest frequency. A successful design for this condition yields a control law which satisfies our stability criteria for all other locations in all three axes. This worst-case point represents x -axis motion when the handle is in the neighborhood of $x = 40$ mm, $y = 150$ mm, $z = 200$ mm, measured from the lower-left-bottom position as seen in Fig. 1. Details on the Excalibur model can be found in [4].

The internal dynamics of the system can be represented in standard second-order form

$$M\ddot{q}(t) + D\dot{q}(t) + Kq(t) = Gu(t) \quad (3)$$

where M , D , and K are the mass, damping, and stiffness matrices, respectively. G is the control distribution matrix. The vector q represents the internal state of the system. u is the input vector

$$u(t) = [f_h(t) \quad f_a(t)]^T. \quad (4)$$

f_h is the force applied at the handle by the human operator in the x -direction. f_a is the force generated by the actuator along the x -axis. The outputs of interest are velocity at the handle, v_h , velocity of the actuator, v_a , and force measured by a strain gauge built into the handle, f_s

$$\begin{bmatrix} v_h(t) \\ -v_a(t) \end{bmatrix} = C_v \dot{q}(t) \quad (5)$$

$$f_s(t) = C_f q(t). \quad (6)$$

The final element to consider is an analog filter, $a(s)$, integrated into the load cell by the manufacturer for noise reduction and anti-aliasing. The output of this filter is the measured force at the handle, f_m . This force measurement and the actuators are non-collocated. The equations governing the dynamics of the system can be written in Laplace form

$$\begin{bmatrix} v_h(s) \\ -v_a(s) \end{bmatrix} = C_v s(Ms^2 + Ds + K)^{-1} G \begin{bmatrix} f_h(s) \\ f_a(s) \end{bmatrix} \quad (7)$$

$$f_m(s) = a(s)C_f(Ms^2 + Ds + K)^{-1} G \begin{bmatrix} f_h(s) \\ f_a(s) \end{bmatrix}. \quad (8)$$

Numerical values, derived from a lumped mass model, for all relevant parameters are provided in the Appendix. The equations of motion can alternatively be written in terms of individual transfer functions

$$\begin{bmatrix} v_h(s) \\ -v_a(s) \end{bmatrix} = \begin{bmatrix} Y_{hh}(s) & Y_{ha}(s) \\ Y_{ah}(s) & Y_{aa}(s) \end{bmatrix} \begin{bmatrix} f_h(s) \\ f_a(s) \end{bmatrix} \quad (9)$$

$$f_m(s) = \begin{bmatrix} F_{mh}(s) & F_{ma}(s) \end{bmatrix} \begin{bmatrix} f_h(s) \\ f_a(s) \end{bmatrix}. \quad (10)$$

Note that two subscripts are attached to each transfer function. The first one matches the subscript of the corresponding output variable. The second subscript matches that of the input variable.

IV. HAPTIC INTERFACE DESIGN

The haptic interface is more than just the mechanical device. It encompasses everything that comes between the human operator and the virtual environment. To better understand the stability properties of the system, we separate the haptic interface into a cascade combination of two subnetworks. These are the

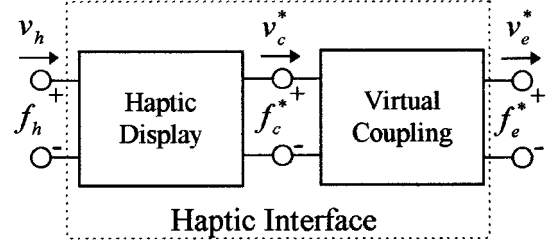


Fig. 4. Haptic interface two-port.

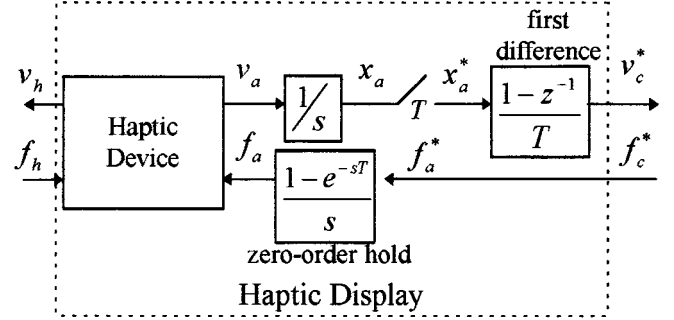


Fig. 5. Impedance display implementation.

haptic display two-port and the virtual coupling two-port, as shown in Fig. 4.

A. Haptic Display Implementations

The haptic display includes the physical structure of the manipulator, as well as actuators, sensors, analog filters, amplifiers, digital-to-analog/analog-to-digital conversion, digital filtering, and control software. There are two ports by which the haptic display can be accessed. At one end there is a physical port, the handle, at which the human operator exchanges energy with the display. At the other end is an information port, characterized by the discrete variables, velocity, v_c^* , and force, f_c^* . Unlike the physical port, a specific causality must be associated with the information port. There are two possibilities. The haptic display can “measure motion and display force” or it can “measure force and display motion” [13], [20]. The former case is an *impedance display*, v_c^* is an output and f_c^* is an input. The latter case is an *admittance display*, v_c^* is an input and f_c^* is an output.

Within the individual classes of impedance and admittance type haptic displays, a number of implementations are possible. Two of the most common will be described here. A third implementation, impedance display with force compensation, is addressed in [21]. It is straightforward to follow the examples below to perform design and analysis for other implementations.

1) *Impedance Display*: This is by far the most common implementation of a haptic display. Either optical encoders or potentiometers provide a measure of device position, x_a , at the point of actuation. This signal is sampled with period T to create the digital signal, x_a^* . The device velocity is estimated, in our case using a simple first difference approximation, to generate the output variable, v_c^* . The digital force command, f_c^* , is passed through a zero-order hold to provide the control input to the actuators. Fig. 5 shows the impedance display implementation. The two-port equations for the haptic display can be derived

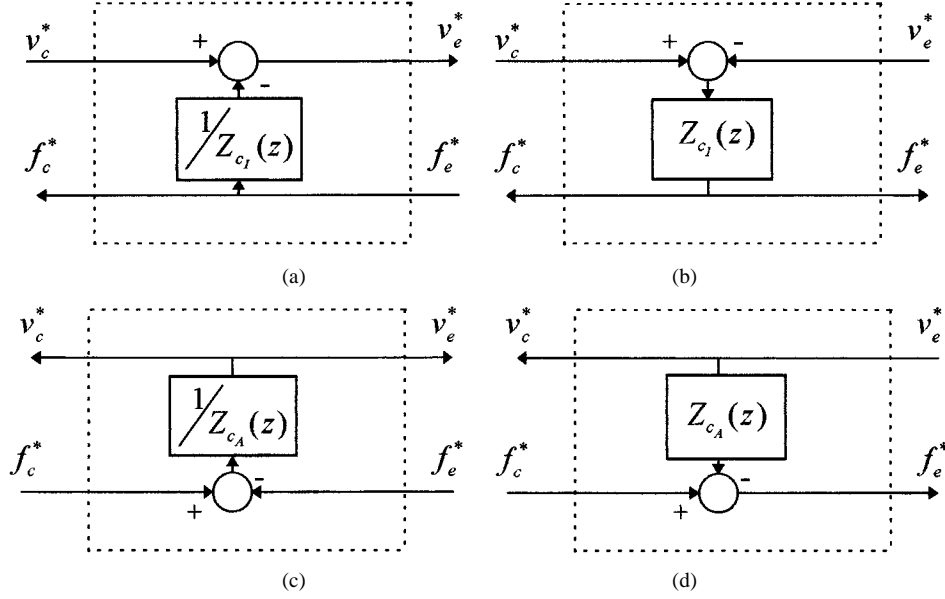


Fig. 7. Virtual coupling implementations.

of these networks to specific topologies, explicit design criteria for the coupling function can be found [13].

For impedance displays, we will consider a two-port with a single shunt impedance

$$Z_{c_I}(z) = b_{c_I} + k_{c_I}Tz/(z-1). \quad (20)$$

This impedance display virtual coupling induces a limit on the maximum impedance which can be rendered. In effect, it acts a spring-damper placed between the virtual environment and the haptic display. It never allows the virtual environment to drive the system unstable by generating an excessively rigid constraint. For performance, we would like the magnitude of $Z_{c_I}(z)$ to be as large as possible, while maintaining the absolute stability of the haptic interface.

For admittance displays, we will limit the virtual coupling two-port to consist of a single series impedance

$$Z_{c_A}(z) = \frac{m_{c_A}b_{c_A}(z-1)}{(m_{c_A} + b_{c_A}T)z - m_{c_A}}. \quad (21)$$

While the virtual environment may simulate an infinitesimally small mass, there is a limit to what the haptic display can

stably render. The admittance display virtual coupling acts as a frequency-dependent damper, providing the required level of impedance to stabilize the system. For performance, we would like $Z_{c_A}(z)$ to be as small as possible, permitting unconstrained free motion, while still meeting the requirements for absolute stability. Further details on the motivation for these virtual couplings are found in [13].

The actual implementation of the virtual coupling networks is dictated by the type of haptic display and virtual environment used in a simulation. At one end, the virtual coupling two-port must match the causality of the haptic display. If an impedance display is used, the coupling must accept velocities, v_c^* , and generate forces, f_c^* . The inverse is true if the coupling is connected to an admittance display. On the other end the virtual coupling two-port must match the causality of the virtual environment. It is possible for a virtual environment to act as an impedance, $f_e^* = Z_e v_e^*$, or as an admittance, $v_e^* = Y_e f_e^*$ [13], [17]. The four possible virtual coupling implementations are shown in Fig. 7.

C. Design for Absolute Stability

1) *Impedance Display—Basic*: When we combine the impedance display implementation with an appropriate virtual

$$\begin{aligned} \begin{bmatrix} v_h(s) \\ f_c^*(s) \end{bmatrix} &= \begin{bmatrix} Y_{hh}(s) - \frac{X_{ha}(s)K_p(e^{sT})X_{ah}^*(s)}{1 + X_{aa}^*(s)K_p(e^{sT})} & \frac{X_{ha}(s)K_p(e^{sT})}{1 + X_{aa}^*(s)K_p(e^{sT})} \left(\frac{T}{1 - e^{-sT}} \right) \\ F_{mh}^*(s) - \frac{F_{ma}^*(s)K_p(e^{sT})X_{ah}^*(s)}{1 + X_{aa}^*(s)K_p(e^{sT})} & \frac{F_{ma}^*(s)}{1 + X_{aa}^*(s)K_p(e^{sT})} \left(\frac{T}{1 - e^{-sT}} \right) \end{bmatrix} \begin{bmatrix} f_h(s) \\ -v_c^*(s) \end{bmatrix} \\ &= \begin{bmatrix} G_{hh}(s) & G_{hc}(s) \\ G_{ch}^*(s) & G_{cc}^*(s) \end{bmatrix} \begin{bmatrix} f_h(s) \\ -v_c^*(s) \end{bmatrix}. \end{aligned} \quad (19)$$

coupling network, Fig. 7(a) or (b), we get the admittance matrix for the combined haptic interface

$$\begin{bmatrix} v_h(s) \\ -v_e^*(s) \end{bmatrix} = \left[\begin{array}{c|c} Y_{hh}(s) & Y_{hc}(s) \\ \hline Y_{ch}^*(s) & Y_{cc}^*(s) + \frac{1}{Z_{c_I}(e^{sT})} \end{array} \right] \cdot \begin{bmatrix} f_h(s) \\ f_e^*(s) \end{bmatrix}. \quad (22)$$

Note that (22) is invariant to the choice of virtual environment causality and thus so are the analysis and design results which follow [13]. The difference lies only in the implementation of the virtual coupling. By applying (1) and (2) to (22), we get the conditions for absolute stability of the haptic interface

$$\operatorname{Re}(Y_{hh}(s)) \geq 0 \quad (23)$$

$$\begin{aligned} 2 \operatorname{Re}(Y_{hh}(s)) \operatorname{Re}(Y_{cc}^*(s) + 1/Z_{c_I}(e^{sT})) \\ \geq |Y_{hc}(s)Y_{ch}^*(s)| + \operatorname{Re}(Y_{hc}(s)Y_{ch}^*(s)). \end{aligned} \quad (24)$$

By definition, $Y_{hh}(s)$ is the transfer function from force applied at the handle to velocity at the handle when the force of actuation is zero. Since the unpowered mechanical device is inherently passive, this open loop admittance function will always be positive real and thus (23) is satisfied without further consideration. The (24) can be rewritten to get an explicit expression which separates the unknown quantities (virtual coupling impedance) from known quantities (haptic display two-port parameters)

$$\operatorname{Re}(1/Z_{c_I}(e^{sT})) \geq \frac{|Y_{hc}(s)Y_{ch}^*(s)| + \operatorname{Re}(Y_{hc}(s)Y_{ch}^*(s))}{2 \operatorname{Re}(Y_{hh}(s)) - \operatorname{Re}(Y_{cc}^*(s))}. \quad (25)$$

This is the virtual coupling design equation. The right side is a real valued function which can be plotted against frequency for $0 \leq \omega \leq \pi/T$. To achieve an absolutely stable haptic interface, we must choose the virtual coupling such that the real part of its admittance function exceeds the lower bound formed by this plot. To maximize performance, we want to maximize virtual coupling impedance. The best performing, absolutely stable solution is achieved by selecting the spring constant, k_{c_I} , and damping, b_{c_I} , which minimize the difference between the left and right hand side of (25) under the constraint that the inequality is satisfied. These values can be found by performing a rapid two-dimensional numerical search.

2) *Admittance Display*: Taking the cascade combination of the admittance display two-port (19) and a single series impedance virtual coupling gives us the alternate hybrid form of the haptic interface equations

$$\begin{bmatrix} v_h(s) \\ f_e^*(s) \end{bmatrix} = \left[\begin{array}{c|c} G_{hh}(s) & G_{hc}(s) \\ \hline G_{ch}^*(s) & G_{cc}^*(s) + Z_{c_A}(e^{sT}) \end{array} \right] \begin{bmatrix} f_h(s) \\ -v_e^*(s) \end{bmatrix}. \quad (26)$$

The absolute stability equations for this case are

$$\operatorname{Re}(G_{hh}(s)) \geq 0 \quad (27)$$

$$\begin{aligned} \operatorname{Re}(Z_{c_A}(e^{sT})) \geq \frac{|G_{hc}(s)G_{ch}^*(s)| + \operatorname{Re}(G_{hc}(s)G_{ch}^*(s))}{2 \operatorname{Re}(G_{hh}(s))} \\ - \operatorname{Re}(G_{cc}^*(s)). \end{aligned} \quad (28)$$

There are two control design steps for the admittance display case:

- First, the position regulator, $K_p(e^{sT})$, is chosen such that $G_{hh}(s)$ is a positive real function.

In other words, the handle of the regulated device must behave passively when the virtual environment velocity is zero. It turns out that we already have developed a way of designing such a regulator. The haptic interface equation for the impedance display, (22), can be rewritten in alternate hybrid form (we are only concerned with the upper left term)

$$\begin{bmatrix} v_h(s) \\ f_e^*(s) \end{bmatrix} = \left[\begin{array}{c|c} Y_{hh}(s) - \frac{\frac{1}{T}(1 - e^{-sT})Z_{c_I}(e^{sT})X_{ha}(s)X_{ah}^*(s)}{1 + \frac{1}{T}(1 - e^{-sT})Z_{c_I}(e^{sT})X_{aa}^*(s)} & - \\ \hline - & - \end{array} \right] \cdot \begin{bmatrix} f_h(s) \\ -v_e^*(s) \end{bmatrix}. \quad (29)$$

Notice that if we make a substitution, $1/T(1 - e^{-sT})Z_{c_I}(e^{sT}) \rightarrow K_p(e^{sT})$, the upper left term becomes $G_{hh}(s)$. Thus, finding $Z_{c_I}(e^{sT})$ which satisfies (25) defines a regulator which forces the upper left term in (29) to be positive real. Once the impedance display virtual coupling is found, the position regulator follows:

$$K_p(e^{sT}) = \frac{1}{T}(1 - e^{-sT})Z_{c_I}(e^{sT}) = k_{c_I} + b_{c_I} \frac{1}{T}(1 - e^{-sT}) \quad (30)$$

which satisfies (27).

- Second, the admittance display virtual coupling function, $Z_{c_A}(z)$, is chosen to satisfy (28).

This entails plotting the right side of (28) and choosing m_{c_A} and b_{c_A} such that the graph of the left side exceeds that curve for all frequencies, $0 \leq \omega \leq \pi/T$. For best performance in this case, we want to minimize the impedance of the virtual coupling. The parameters are selected to minimize the difference between the left and right sides of (28) under the constraint that the inequality is satisfied.

3) *Impact of Human Model on Stability Condition*: For Excalibur, we assume human arm impedance to be bounded by $Z_{\max}(s) = 300 + 1000/s$ N/(m/s), corresponding to a stiffness of 1000 N/m and a damping of 300 N/(m/s). These values are consistent with previous work [25] as well as with experimental measurements taken by the authors. We do not limit the minimum impedance imparted by the human, $Z_{\min} = 0$. While the linear human impedance bound may be simplistic for frequencies below 5 Hz, it is assumed the human operator does not deliberately attempt to destabilize the system. In fact, one may argue the haptic display should not attempt to stabilize “unstable” motion deliberately induced by the operator. The limit on maximum human operator impedance may be included in the stability analysis by simply replacing $Y_{hh}(s) \rightarrow Y_{hh}(s) + 1/Z_{\max}(s)$ in all of the preceding equations.

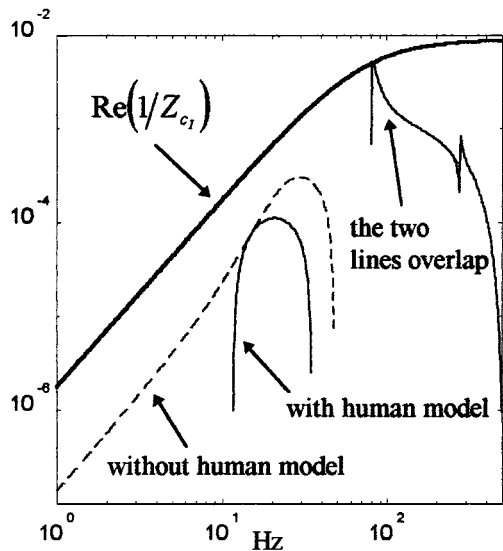


Fig. 8. Impedance display virtual coupling design.

V. NUMERICAL AND EXPERIMENTAL RESULTS

Control laws have been designed for Excalibur for the two haptic display implementations described above. The worst-case configuration, detailed in the Appendix, is the focus of the numerical design. The resulting regulators and virtual couplings have been implemented in software and tested on Excalibur as part of the VBB system. The VBB environment has admittance causality, so virtual couplings are implemented as shown in Fig. 7(b) or (d).

A. Impedance Display

We use (25) to find a virtual coupling of the form (20) which makes the haptic interface absolutely stable. The lower bound formed by the right side of (25) is shown as a dashed line in Fig. 8. The line disappears at some frequencies when the bound becomes negative. When the haptic interface equations are modified to include the human operator impedance model, the resulting design bound is shown as a thin solid line in Fig. 8. At frequencies above 70 Hz, there is little difference between these two curves, and there is no difference in the resulting control design. Using the design bound the best performing, absolutely stabilizing virtual coupling parameters, k_{c_I} and b_{c_I} , are found. The left side of (25) with the resulting values, $k_{c_I} = 51\,000$ N/m and $b_{c_I} = 90$ N/(m/s), is plotted on Fig. 8 as a bold line.

B. Admittance Display

The first step in control law design for the admittance display implementation was accomplished when we found the impedance display virtual coupling parameters. Following (30), the position regulator is

$$K_p(e^{sT}) = 51\,000 + 90 \frac{1}{T} (1 - e^{-sT}) \text{ N/m.} \quad (31)$$

The second step is to use (28) to find a virtual coupling which provides absolute stability. Fig. 9 shows the lower bound on the real part of virtual coupling impedance. The dashed line is the bound calculated without a human impedance model. The thin solid line shows the bound modified to include a limit on

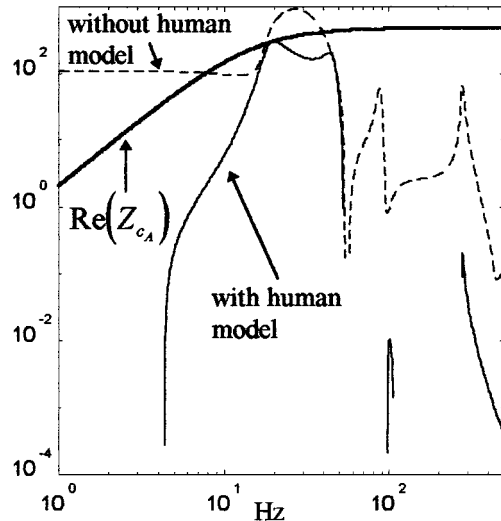


Fig. 9. Admittance display virtual coupling design.

maximum human impedance. Here we see that the virtual coupling design is dramatically affected by the introduction of the human model. Conservatism induced by allowing unreasonable levels of human interaction drives the required virtual coupling impedance to excessive levels. The virtual coupling designed using the human model is represented by the bold line in Fig. 9. The corresponding virtual coupling parameters which define $Z_{c_A}(e^{sT})$ in (21) are $b_{c_A} = 500$ N/(m/s) and $m_{c_A} = 5.0$ kg. We should note that the position regulator in (31) represents the “stiffest” allowable controller. These gains may be reduced, which in turn allows reduced impedance in the virtual coupling. The tradeoff between regulator gain and virtual coupling impedance is explored further, later in the paper.

C. Experimental Results

The control laws for the different haptic display implementations have been tested on the VBB system. This simulation falls under the class of admittance type virtual environments. The virtual world consists of a cursor and up to 50 building blocks. By default, the virtual coupling connects the haptic display to the cursor. When the cursor is moved inside a block and a mouse button clicked, the device “grabs” that block, connecting the virtual coupling to it. When a selected block collides with another block or blocks in the virtual environment, its position is constrained to lie on the surface of the obstruction. The blocks may also be vertically mated together by aligning their knobs and overcoming inter-block friction. The equations of motion are integrated using an Euler velocity approximation and a trapezoidal position estimate. As noted by Brown and Colgate [17], since an explicit integration routine is used, the virtual environment does not strictly satisfy discrete-time passivity. The implication here is that we cannot simulate an infinitesimally small mass while maintaining a stable numerical integration of the equations of motion. The experimentally determined minimum value for cursor and block masses is 0.25 kg. Under this condition, both of the control designs described above provide a stable haptic simulation. We use the term stable here to imply that there are no detectable undamped or divergent oscillations under any combination of virtual environment state

TABLE I
THEORETICAL VERSUS EXPERIMENTAL STABILITY BOUNDARY GAINS

	Impedance		Admittance	
	k_{c_1}	b_{c_1}	m_{c_A}	b_{c_A}
Theoretical	51,000	90	5.0	500
Experimental	75,000	90	4.3	500

and human operator grasp. The important virtual environment states are: free motion, unilateral block–block collision, and bilaterally constrained block. Possible human operator grasp conditions are: hands-off, relaxed operation, and tight grip with arm fully extended. The first condition corresponds to zero human impedance, the last to maximum grasp impedance.

The control parameters were tuned to find the values which make the system marginally stable. Table I shows these experimentally derived stability boundary gains along with their theoretical counterparts. For the impedance display virtual coupling, damping was held constant and stiffness increased until instability was first detected. This occurred when the value was augmented by 50% in the virtual environment/human operator combination of bilateral constraint/hands-off. The experimental admittance display virtual coupling was found by reducing the mass while holding constant the theoretical damping and position regulator gains. Instability occurred in the combination of free-motion/maximum grasp when the mass was reduced by 15%.

A number of factors may account for the difference between theoretical and experimental results. The theoretical control laws are based on a linear model of Excalibur. Any discrepancy between this model and the true system’s behavior will lead to design error. In addition to any error in the linear model, nonlinearities are not accounted for in the design. Certainly, effects such as motor cogging torque and transmission cable slack contribute to the difference. Finally, while our experiments attempt to consider worst-case combinations of virtual environment state/human grasp impedance, they by no means comprise an exhaustive search of all allowable port impedances. If the tests missed the true worst-case scenario, the experimental results may be optimistic. Without an exhaustive search of all possible terminating impedance combinations, it will always be possible the worst-case scenario was missed. While the experimental gains achieved better performance than the theoretical values, they put the system on the edge of oscillation and did not provide the user with an ideal kinesthetic response. During practical use of the VBB system, the theoretical gains were normally used to provide a robustness margin against oscillations.

D. Performance Comparison

Quantifying the performance of a haptic interface can be difficult, since our ultimate goal has to do with human perception. We want the interface to act as a transparent window into

the virtual environment. When the virtual environment simulates free motion, such as free cursor motion in the VBB simulation, the human operator should feel zero (or very small) force at the handle. Ideally, the operator would not even realize that the handle was there. When the virtual environment simulates zero velocity, such as when a selected building block is “stuck” between other objects, the handle should be immobile. One way of quantifying haptic interface performance is the notion of impedance range [7]. The impedance range is delineated by the minimum and maximum impedance which the haptic interface can *stably* render to the human operator. If the haptic interface is absolutely stable, then it is straightforward to calculate these bounds on realizable impedance. The minimum impedance is simply the input impedance at the human operator port with the virtual environment port short-circuited

$$Z_{\min}(s) = \left. \frac{f_h(s)}{v_h(s)} \right|_{f_e^*(s) \rightarrow 0} \quad (32)$$

The maximum impedance is found with an open-circuit virtual environment

$$Z_{\max}(s) = \left. \frac{f_h(s)}{v_h(s)} \right|_{v_e^*(s) \rightarrow 0} \quad (33)$$

The magnitude of the impedance range bounds for the two haptic display implementations considered in this paper are shown in Fig. 10(a). The thin lines represent the impedance display and the bold lines show the admittance display bounds. The frequency responses are calculated using the worst-case design model and the theoretical control laws.

The lower bound represents the free-motion response of the haptic interface. For the impedance display, this is simply the open-loop response of the system. Below 10 Hz, this response is dominated by rigid body damping [20 N/(m/s)] and the total inertia (3.9 kg). The lower bound for the admittance display implementation is driven by the virtual coupling impedance. At frequencies below 10 Hz, the response is dominated by the coupling mass of 5.0 kg. In this case, the operator “feels” greater inertia than in the impedance implementation, but with zero damping. When the virtual environment simulates free motion, the handle literally floats around the workspace like a frictionless mass.

The upper bound on impedance range represents the handle impedance when the virtual environment simulates an infinitely rigid constraint. Below 10 Hz, the haptic interface acts as a grounded spring, $Z_{\max}(s) \approx k/s$. For an impedance display implementation, the effective spring constant, 20 000 N/m, is the series combination of virtual coupling stiffness and mechanical stiffness between the handle and the actuators. The effective spring constant for the admittance display is the series combination of the position regulator’s stiffness (gain on displacement) and the device mechanical stiffness. Its value is also 20 000 N/m. Since we chose the admittance display position regulator gains to be the same as the impedance display virtual coupling gains, these two cases have identical upper bounds.

We have described in some detail two different realizations of a haptic interface. Both are implemented on the same hardware, both are absolutely stable, and both can be connected to an impedance or admittance type virtual environment. The obvious

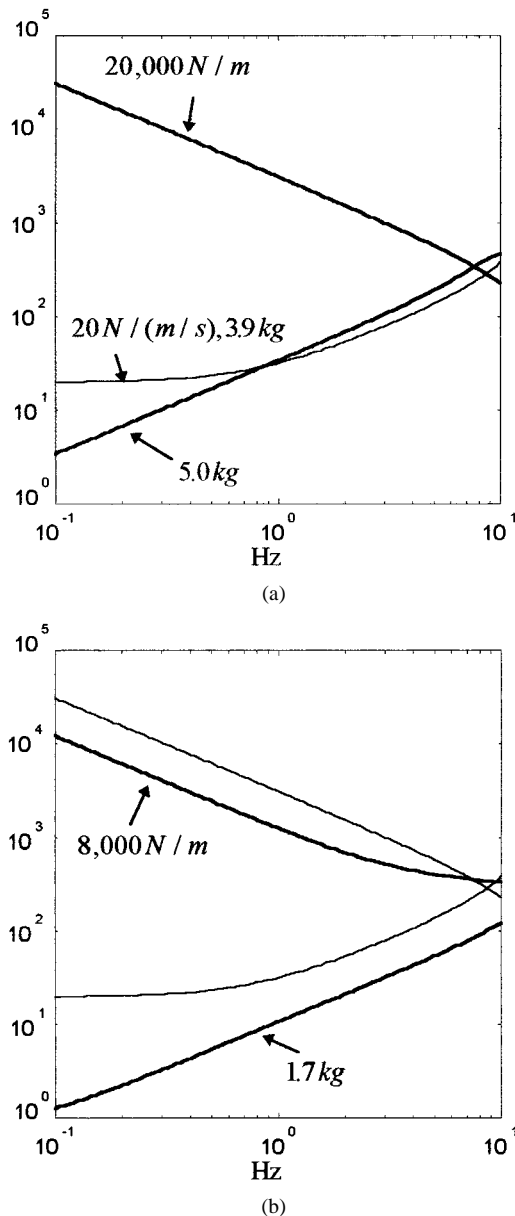


Fig. 10. Impedance range for different haptic display implementations (thin line—impedance display, bold line—admittance display).

question is: Which is best? In general, the answer is device dependent. The impedance display is the simplest implementation (no force sensor is required), but is also the least adaptable. It is difficult to improve the free-motion response of the display beyond the backdrivability of the open-loop device. For a device which is lightweight and with low-friction, this may be the best implementation. The admittance display implementation is tailorable, and is likely the best implementation for a device which has high levels of nonlinear friction and high gear ratios.

The ability to tailor the performance of the admittance display is highlighted in Fig. 10(b). By reducing the inner loop position gain to 10 000 N/m, the virtual coupling impedance parameters can be reduced to $b_{c_A} = 450 \text{ N/(m/s)}$ and $m_{c_A} = 1.5 \text{ kg}$ while still providing absolute stability. The new impedance range bounds show the corresponding improvement in free-motion response (1.7 kg) and degradation in rigid-constraint performance (8000 N/m).

VI. CONCLUSION

Two-port absolute stability criteria have been developed for the design of stabilizing haptic interface control laws for a wide range of human operator and virtual environment impedance. The approach has been demonstrated in the design of regulators and virtual couplings for two different haptic display implementations: impedance display and admittance display. Numerical and experimental results for the Excalibur device have validated the efficacy of the theoretical methods.

APPENDIX

The worst-case design model for Excalibur is defined in terms of the matrices, M , D , K , G , C_v , and C_f . This model characterizes the local behavior of the device along the x -axis at its point of maximum flexibility. See equations (34)–(39) shown at the top of the next page. The analog filter on load cell output is

$$a(s) = \frac{235}{s + 235}. \quad (40)$$

REFERENCES

- [1] C. V. Edmond *et al.*, "ENT endoscopic surgical training simulator," *Proc. Medicine Meets Virtual Reality*, pp. 518–528, 1997.
- [2] R. Baumann and R. Clavel, "Haptic interface for virtual reality based minimally invasive surgery simulation," in *Proc. IEEE Int. Conf. Robot. Automat.*, 1998, pp. 381–386.
- [3] C. J. Hasser, "User performance in a GUI pointing task with a low-cost force-feedback computer mouse," in *Proc. ASME Int. Mechanical Eng. Congr. Exhibition*, Anaheim, CA, 1998.
- [4] R. J. Adams, M. R. Moreyra, and B. Hannaford, "Excalibur, A three-axis force display," in *Proc. ASME Symp. Haptic Interfaces*, vol. DSC-Vol. 67, Nashville, TN, 1999, pp. 289–296.
- [5] R. Adams, D. Klowden, and B. Hannaford, "Stable haptic interaction using the excalibur force display," in *Proc. IEEE Int. Conf. Robot. Automat.*, San Francisco, CA, April 2000.
- [6] B. Hannaford, "A design framework for teleoperators with kinesthetic feedback," *IEEE Trans. Robot. Automat.*, vol. 5, pp. 426–434, 1989.
- [7] J. E. Colgate and J. M. Brown, "Factors affecting the Z-width of a haptic display," in *Proc. IEEE Int. Conf. Robot. Automat.*, Los Alamitos, CA, 1994, pp. 3205–3210.
- [8] M. Minsky, M. Ouh-Young, O. Steele, F. P. Brooks, and M. Behensky, "Feeling and seeing issues in force display," *Comput. Graphics*, vol. 24, no. 2, pp. 235–243, 1990.
- [9] J. E. Colgate, P. E. Grafing, M. C. Stanley, and G. Schenkel, "Implementation of stiff virtual walls in force-reflecting interfaces," in *Proc. IEEE Virtual Reality Annu. Int. Symp.*, Seattle, WA, 1993, pp. 202–208.
- [10] S. E. Salcudean and T. D. Vlaar, "On the emulation of stiff walls and static friction with a magnetically levitated input/output device," *Trans. ASME, J. Dyn. Syst., Measurement, Contr.*, vol. 119, pp. 127–132, 1997.
- [11] J. E. Colgate, M. C. Stanley, and J. M. Brown, "Issues in the haptic display of tool use," in *Proc. IEEE/RSJ Int. Conf. Intell. Robot. Syst.*, Pittsburgh, PA, 1995, pp. 140–145.
- [12] C. B. Zilles and J. K. Salisbury, "A constraint-based God-object method for haptic display," in *Proc. IEEE/RSJ Int. Conf. Intell. Robot. Syst.*, Pittsburgh, PA, 1995, pp. 146–151.
- [13] R. J. Adams and B. Hannaford, "Stable haptic interaction with virtual environments," *IEEE Trans. Robot. Automat.*, vol. 15, pp. 465–474, 1999.
- [14] S. K. Mitra, *Analysis and Synthesis of Linear Active Networks*, New York: Wiley, 1969.
- [15] F. B. Llewellyn, "Some fundamental properties of transmission systems," *Proc. IRE*, vol. 40, pp. 271–283, 1952.
- [16] N. Hogan, "Controlling impedance at the man/machine," in *Proc. IEEE Int. Conf. Robot. Automat.*, Scottsdale, AZ, 1989, pp. 1626–1631.
- [17] J. M. Brown, "Passive implementation of multibody simulations for haptic display," Doctoral dissertation, Mech. Eng., Northwestern Univ., Evanston, IL, Dec. 1998.
- [18] J. M. Brown and J. E. Colgate, "Passive implementation of multibody simulations for haptic display," in *Proc. ASME Int. Mech. Eng. Congr. Exhibition*, Dallas, TX, 1997, pp. 85–92.

$$M = \begin{bmatrix} 0.9271 & 0 & 0 & 0 & 0 \\ 0 & 0.3875 & 0 & 0 & 0 \\ 0 & 0 & 2.4489 & 0.2799 & 0 \\ 0 & 0 & 0.2799 & 0.3343 & 0 \\ 0 & 0 & 0 & 0 & 0.1600 \end{bmatrix} \quad (34)$$

$$D = \begin{bmatrix} 8.5600 & -2.7895 & -1.1447 & 0.0487 & 0.0095 \\ -2.7895 & 12.2139 & -7.4320 & 0.0529 & -0.0551 \\ -1.1447 & -7.4320 & 68.2359 & 48.6630 & -47.4150 \\ 0.0487 & 0.0529 & 48.6630 & 49.2727 & -47.3653 \\ 0.0095 & -0.0551 & -47.4150 & -47.3653 & 48.2606 \end{bmatrix} \quad (35)$$

$$K = 10^7 \cdot \begin{bmatrix} 0.0236 & -0.0280 & 0.0045 & -0.0003 & -0.0001 \\ -0.0280 & 0.1044 & -0.0764 & 0.0000 & 0.0000 \\ 0.0045 & -0.0764 & 5.3954 & 5.3238 & -5.3235 \\ -0.0003 & 0.0000 & 5.3238 & 5.3270 & -5.3235 \\ -0.0001 & 0.0000 & -5.3235 & -5.3235 & 5.3236 \end{bmatrix} \quad (36)$$

$$G = \begin{bmatrix} 0 & -1 \\ 0 & 0 \\ 0 & 0 \\ 0 & 0 \\ 1 & 0 \end{bmatrix} \quad (37)$$

$$C_v = \begin{bmatrix} 0 & 0 & 0 & 0 & 1 \\ -1 & 0 & 0 & 0 & 0 \end{bmatrix} \quad (38)$$

$$C_f = 10^7 \cdot [0 \quad 0 \quad -5.3236 \quad -5.3236 \quad 5.3236]. \quad (39)$$

- [19] R. J. Adams, M. R. Moreyra, and B. Hannaford, "Stability and performance of haptic displays: Theory and experiments," in *Proc. ASME Int. Mech. Eng. Congr. Exhibition*, Anaheim, CA, 1998, pp. 227–234.
- [20] T. Yoshikawa, Y. Yokokohji, T. Matsumoto, and X.-Z. Zheng, "Display of feel for the manipulation of dynamic virtual objects," *Trans. ASME, J. Dyn. Syst., Measurement, Contr.*, vol. 117, no. 4, pp. 554–558, 1995.
- [21] R. J. Adams, "Stable haptic interaction with virtual environments," Doctoral dissertation, Elect. Eng., Univ. Washington, Seattle, WA, Aug. 1999.
- [22] T. H. Massie and J. K. Salisbury, "The phantom haptic interface: A device for probing virtual objects," in *Proc. ASME Int. Mech. Eng. Congr. Exhibition*, Chicago, IL, 1994, pp. 295–302.
- [23] Y. Yokokohji, R. L. Hollis, and T. Kanade, "What you see is what you can feel—Development of a visual/haptic interface to virtual environment," in *Proc. IEEE Virtual Reality Annu. Int. Symp.*, Los Alimitos, CA, 1996, pp. 46–53.
- [24] C. L. Clover, G. R. Luecke, J. J. Troy, and W. A. McNeely, "Dynamic simulations of virtual mechanisms with haptic feedback using industrial robotics equipment," in *Proc. IEEE Int. Conf. Robot. Automat.*, Albuquerque, NM, 1997, pp. 3205–3210.
- [25] F. A. Mussa-Ivaldi, N. Hogan, and E. Bizzi, "Neural, mechanical, and geometric factors subserving arm posture in humans," *J. Neurosci.*, vol. 5, no. 10, pp. 2732–2743, 1985.



Blake Hannaford (S'82–M'84–SM'01) received the B.S. degree in engineering and applied science from Yale University, New Haven, CT, in 1977 and the M.S. and Ph.D. degrees in electrical engineering from the University of California, Berkeley, in 1982 and 1985, respectively.

Before graduate study, he held engineering positions in digital hardware and software design, office automation, and medical image processing. At Berkeley, he pursued thesis research in multiple target tracking in medical images and the control of time-optimal voluntary human movement. From 1986 to 1989, he worked on the remote control of robot manipulators in the Man–Machine Systems Group in the Automated Systems Section of the NASA Jet Propulsion Laboratory, Caltech. He supervised that group from 1988 to 1989. Since September 1989, he has been at the University of Washington, Seattle, where he has been Professor of Electrical Engineering since 1997, and served as Associate Chair for Education from 1999 to 2001. His currently active interests include haptic displays on the Internet, and surgical biomechanics. He is the founding editor of *Haptics-e*, *The Electronic Journal of Haptics Research* (www.haptics-e.org).

Dr. Hannaford was awarded the National Science Foundation's Presidential Young Investigator Award and the Early Career Achievement Award from the IEEE Engineering in Medicine and Biology Society.



Richard J. Adams is a Major in the United States Air Force. He received the B.S. degree from the U.S. Air Force Academy, Colorado Springs, CO, in 1989 as a Distinguished Graduate. In 1990, he received the M.S. degree in aeronautics and astronautics from the University of Washington, Seattle. He received the Ph.D. degree in electrical engineering from the University of Washington in 1999.

He worked from 1991 to 1993 in Wright Laboratory, Dayton, OH on advanced flight controls for fighter aircraft. From 1994 to 1996, he served as an

Exchange Scientist with the C.E.R.T. research center in Toulouse, France.

Major Adams received the Air Force Scientific Achievement Award for his work on F-16 high angle-of-attack control in 1994.